Proceedings of 49th ASME IGTI
ASME Turbo Expo Land, Sea, and Air 2004
June 14-17, 2004; Vienna, Austria

GT2004-53196

MELT-INFILTRATED SIC COMPOSITES FOR GAS TURBINE ENGINE APPLICATIONS

Gregory N. Morscher*
Ohio Aerospace Institute, Cleveland, OH

Vijay V. Pujar
Goodrich Corporation, Brecksville OH

ABSTRACT

SiC-SiC ceramic matrix composites (CMCs) manufactured by the slurry-cast melt-infiltration (MI) process are leading candidates for many hot-section turbine engine components. A collaborative program between Goodrich Corporation and NASA-Glenn Research Center is aimed at determining and optimizing woven SiC/SiC CMC performance and reliability. A variety of composites with different fiber types, interphases and matrix compositions have been fabricated and evaluated. Particular focus of this program is on the development of interphase systems that will result in improved intermediate temperature stressed-oxidation properties of this composite system. The effect of the different composite variations on composite properties is discussed and, where appropriate, comparisons made to properties that have been generated under NASA's Ultra Efficient Engine Technology (UEET) Program.

INTRODUCTION

Silicon carbide fiber reinforced-silicon carbide matrix composites consisting of polycrystalline SiC fiber and matrix processed via melt-infiltration are being pursued for aircraft jet engine components such as combustor liners and vanes [1,2] and for land-based gas-turbine applications such as combustor liners [3] and shrouds [4]. Material development has progressed to a relatively mature status for example, under the NASA Enabling Propusion Materials (EPM) and Ultra Efficient Engine Technology (UEET) programs [1,5]. However, optimization of composite processing, constituent content, and architecture are still required for improved reliability and performance. Goodrich Corporation and NASA Glenn Research Center have entered into a collaborative effort towards that end, by combining the composite processing experience of Goodrich with the microstructure/property understanding of these composite systems learned at NASA.

The composite systems studied at NASA in the past have mostly utilized the Sylramic fiber (Dow Corning). Unfortunately, at the time of this work the Sylramic fiber was not commercially available. Therefore, composites with available high-temperature polycrystalline fiber-types, Hi-Nicalon Type S (Nippon Carbon) and Tyranno SA (Ube Industries), were fabricated. In this paper, these are referred to as HNS and SA, respectively. The baseline system, was based on a relatively low temperature chemical vapor infiltrated (CVI) interphase consisting primarily of BN, which is referred to as LTI. For the HNS system, panels were fabricated from 2D fabric lay-up with LTI and different fractions of matrix constituents, namely, CVI SiC, particulate SiC, and Si. For the SA composites, three additional interphase variations were attempted, all aimed at improving intermediate temperature properties. The first was a high temperature Si-doped BN interphase, referred to hereafter as HTI, which has been evaluated in prior work at NASA on the Sylramic fiber system [6]. The other two variants evaluated in this study were derived by subjecting the LTI and HTI interphases to additional treatment to enable outside debonding, *i.e.*, debonding of the fiber from the matrix between the BN interphase and the CVI-SiC portion of the matrix. The outside debond contrasts with the normally observed "inside debond" where the debonding is between the fiber and the BN. Details of the "outside debond" concept and their potential implications on composite performance have been reported previously for composite systems based on the Sylramic fiber [7]. The outside debond interphase variants attempted in this study are referred to here as LTO and HTO, respectively.

Several tests were performed on each panel to evaluate and compare the different composite systems. These tests were aimed at evaluating a composite system with a view towards the key property needs required for gas turbine hot-section components such as high strengths, both initial and retained after service, good creep and stress-rupture properties over a wide temperature range, and good through-thickness properties [5]. The tests performed were room temperature (with acoustic emission) and elevated temperature fast fracture tensile testing, elevated temperature tensile stress-rupture and creep testing, interlaminar tensile testing, and through-thickness thermal conductivity measurements. At the time of writing this paper, not all of the testing was complete; however, sufficient data is available to make some conclusions on the relative performance of the different composite systems studied.

* Senior Research Scientist residing at NASA Glenn Research Center, Cleveland, OH

EXPERIMENTAL

For the baseline composites consisting of the LTI interphase, composite panels were fabricated as follows: eight 15.2 cm x 15.2 cm plies of five-harness woven fabric were stacked in a 0/90 lay-up and consolidated sequentially with, (1) CVI of the LTI interphase, (2) CVI of SiC matrix overcoat, (3) slurry infiltration of aqueous solution containing α-SiC particles, and (4) molten infiltration of an alloy primarily consisting of Si to near full density. The weight of the woven fabric prior to consolidation was measured as well as after steps (2) through (4).

For composites with the HTI interphase, the interphase was applied by CVI on a 0.3 m by 2 m piece of woven fabric at Synterials Inc. (Herndon, VA). The coated fabric was then cut into 15.2 cm x 15.2 cm pieces. Eight plies were stacked in a 0/90 lay-up and subjected to steps (2) above and following. SA composites, where outside debonding interphases LTO and HTO were attempted, were subjected to the additional processing step prior to step (2) in both cases.

Table 1 lists the physical properties of the fabricated composite panels described in this paper. Some explanation of the method of estimating fiber volume fraction is required. There is always some variation in measured thickness of composite specimens. Since the volume fraction of fibers is the critical constituent parameter for understanding composite strength and there is slight variation in measured thickness from specimen to specimen, the fraction of fibers in the loading direction, f_o, was determined geometrically (Equation 1) from the number of plies, N_{ply}, the number of fibers per tow, N_f (500 for HNS and 800 for SA), the average fiber radius, R_f (6.5 μm for HNS and 5 μm for SA as measured from polished cross-sections), the tow ends per mm, *epmm*, and the thickness of the specimen, *t*.

$$f_o = \frac{N_{ply} N_f \pi R_f^2 (epmm)}{t} \qquad (1)$$

The total volume fraction of fibers in the composite, *f*, is then $2f_o$. For Table 1, the average fraction of fibers was based on the average composite thickness measured for all the specimens tested. Composite thickness varied by as much as 0.1 mm. The thickness of the interphase was based on measured interphase thicknesses from a witness piece of fabric processed during each interphase run. For the HNS composites, the content of the matrix was varied. These are designated by "A" and "B" in Table I. The HNS/LTI-B composite had a significantly greater fraction of melt-infiltrated Si and significantly lower fraction of CVI SiC than the HNS/LTI-A composites.

Table 1: Physical Properties of Composite Panels

Panel	epcm	Avg spec. thickness, mm	Avg. f	Interphase thickness, μm	Panel density, g/cc
HNS/LTI-A1	7.1	2.50	0.30	0.35	2.83
HNS/LTI-A2	7.1	2.17	0.35	0.35	2.74
HNS/LTI-B	7.1	2.29	0.33	0.35	2.79
SA/LTI1	7.9	2.57	0.31	0.35	2.79
SA/LTI2	7.9	2.71	0.29	0.49	2.82
SA/LTO1	7.9	2.00	0.40	0.46	2.73
SA/LTO2	7.9	1.97	0.40	0.46	2.72
SA/HTI	7.9	2.48	0.32	0.50	2.87
SA/HTO1	7.9	2.52	0.31	0.50	2.83
SA/HTO2	7.9	2.31	0.34	0.50	2.80

Room temperature tensile testing was performed on 152 mm tapered "dogbone" specimens. The width at the grip region was 12.6mm whereas the width in the gage section was 10 mm. Tensile-tests were performed using screw-driven universal test machines (Instron Inc.) with pneumatic "wedge" grips. The grip-ends of the specimens were wrapped with a metal wire-mesh screen. Contact extensometers with a 25 mm span were used to measure displacement. Three acoustic emission (AE) sensors were attached with spring clamps along the length as shown in Figure 1. The center AE sensor was placed at the center of the gage section and the distance from the center AE sensor to the upper or lower sensor was 25 mm.

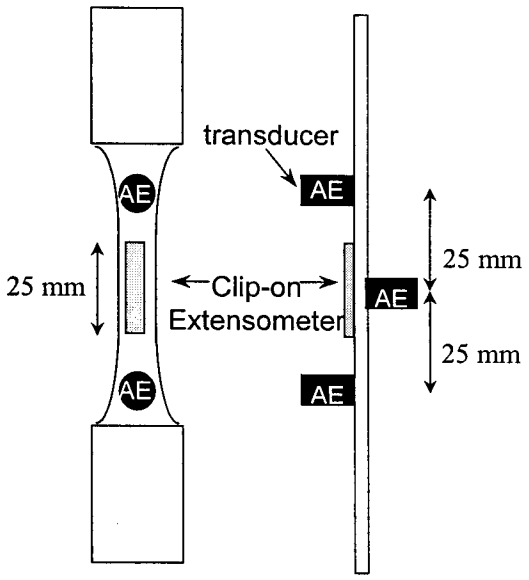

Figure 1: Schematic representation of AE sensor placement.

Therefore, events that triggered the center sensor first came from the gage section. The AE generated in the gage section was the only AE data used for analysis of composite behavior.

Elevated temperature testing was performed at 815°C and 1315°C. The specimens were gripped in water-cooled wedge-grips. A $MoSi_2$ element, resistance-heated furnace was inserted in between the two grips, the hot zone was approximately 15 mm. Fast fracture testing was performed at 1315°C. Stress-rupture tests were performed at 815°C. If a specimen survived 100 hours or more at 815°C, a fast-fracture test was performed at temperature to determine the retained strength of the composite. Creep tests were performed at 1315°C at 103 MPa for 100 hours. After the 100 hours, a fast-fracture test was performed at temperature in order to determine the retained strength.

Microscopy was performed on tested specimens. Several fracture surfaces were examined with a field emission scanning electron microscope, FESEM, (Hitachi Model 4700). Most of the specimens were cut and polished length-wise in order to observe the extent of matrix cracking. Fast-fracture tested composite specimens usually required a plasma-etch (CF4 plasma at 500 W for 30 minutes) in order to observe the matrix cracks. Since the plasma-etch usually removed the Si at the surface of the polished specimen matrix cracks could be

observed only through the CVI SiC portion of the matrix. Stress-rupture tested specimens usually had matrix cracks that were very easy to observe since oxidation at the interphase resulted in large matrix crack openings.

Through-thickness properties were also determined. Interlaminar tensile strengths were measured using a 2.54 cm "button" test. Through-thickness thermal conductivity was determined from measurements of thermal diffusivities and specific heat from room temperature to 1000°C [8].

RESULTS AND DISCUSSION

Room Temperature Tensile Properties

Typical room temperature tensile-hysteresis stress-strain curves are shown in Figure 2 for a HNS/LTI composite. Note that the composite stiffens upon unloading, typical of MI composites with high-modulus SiC fibers, due to a net compressive stress in the matrix. The intersection of the average hysteresis modulus taken from the upper part of the hysteresis estimates the residual compressive stress in the composite [9]. Also plotted in Figure 2 is the normalized

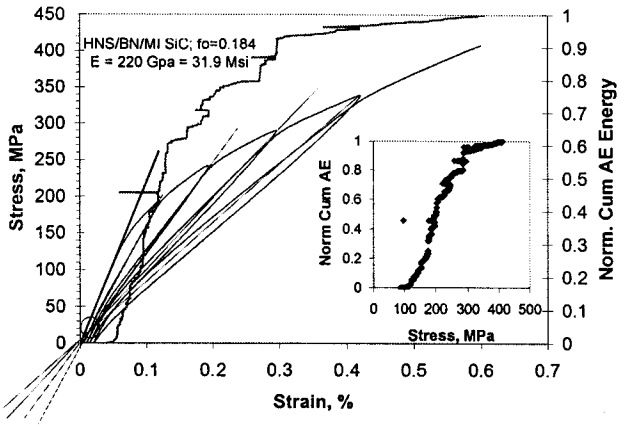

Figure 2: Room temperature stress-strain and AE behavior for HNS/LTI-A2.

cumulative AE energy versus strain. The normalized cumulative AE energy versus applied stress is shown in the inset in Figure 2. The normalized cumulative AE energy has been shown to be proportional to matrix crack formation and propagation [10].

The stress-strain behavior and AE activity for all the composites are shown in Figure 3. Note that the HNS composites had higher stresses and strains to failure at room temperature than the SA composites. The variation in stress-strain behavior for the different composite systems is due to the different constituents and constituent contents for each composite panel.

The stress-dependent AE activity for the different composites are shown in the inset in Figure 3. Initial AE activity occurred between 75 and 129 MPa for the different composite systems tested. The onset of high-energy AE activity, which corresponds to the formation of large, usually through-thickness, matrix cracks ranged from 120 to 166 MPa for the different composites tested.

The room temperature properties for all of the composites are summarized in Table 2. The elastic modulus was determined from the linear-regression fit of the 0 to 50 MPa portion of the stress-strain curve. The "proportional limit" was determined where the linear-regression fit elastic modulus

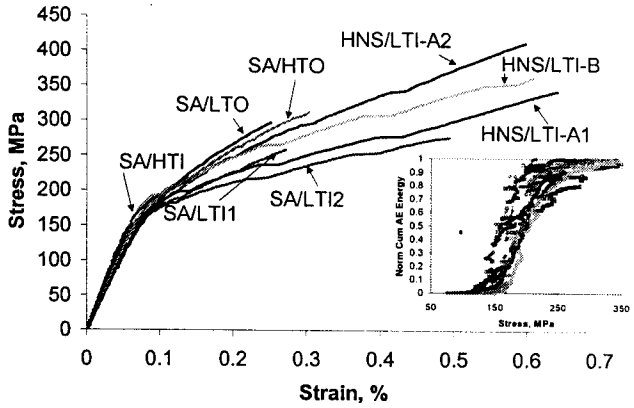

Figure 3: Stress-strain behavior (hysteresis loops removed) and AE activity versus stress (inset) for all the composites.

Table 2: Room Temperature Mechanical Properties

Panel	f	E, GPa	RT Ult. Stress, MPa	RT Ult. Strain, %	Residual stress, MPa	ρ_c, mm^{-1}	τ, MPa	0.002% Offset Stress, MPa
HNS/LTI-A1	0.30	262	349	0.64	-22	7	36	135
HNS/LTI-A2	0.35	220	412	0.6	-20	6.7	28	125
HNS/LTI-B	0.33	270	362	0.61	-40	7.6	38	151
SA/LTI1	0.30	274	256	0.274	-22	5.8	48	138
SA/LTI2	0.29	242	270	0.47	-15	6.3	22	142
SA/LTO1	0.40	210	293	0.25	-5	7.5	50	126
SA/LTO2	0.40	200	294	0.275	-19	--	--	115
SA/HTI	0.32	259	210	0.14	NA	--	--	140
SA/HTO1	0.31	NA	226	NA	NA	--	--	NA
SA/HTO2	0.34	236	306	0.3	-23	7.5	60	155

curve, displaced by 0.002% in strain, intersects the stress-strain curve.

For the HNS composites, high strengths were achieved. This was especially true when compared to HNS MI composites tested at NASA from a different vendor (e.g., see references 6and 7). When the stress on the fibers at ultimate failure was calculated (ultimate composite stress divided by fraction of fibers in the loading direction), the HNS composites tested in this study averaged 2220 $\pm$ 80 MPa whereas the HNS composites tested in the earlier study from the other vendor averaged 1800 $\pm$ 100 MPa at failure. This may be due to a different lot of fiber.

One other observation of note, the HNS/LTI-B system which had lower CVI SiC content and higher Si content compared to HNS/LTI-A, showed higher compressive residual stress as well as higher 0.002% offset (proportional limit) stress. This can be explained by both the volume expansion of Si upon solidification and the lower thermal expansion coefficient of Si than the SiC fibers. Both of these properties place the "matrix" in compression. Increasing the content of Si

increases the residual compressive stress in the matrix and consequently the matrix cracking stress as well.

For SA composites, more variability was observed in stress-strain behavior; however, much of this could be explained by differences in fiber volume fraction. The strengths of SA composites were lower than HNS composites, which were expected since SA fibers as-produced are weaker than HNS. On average, the strength of SA fibers at failure for the stronger systems, SA/LTI and SA/HTO, was 1780 $\pm$ 80 MPa. The SA/LTO composite panels only averaged 1480 $\pm$ 30 MPa fiber strengths at failure. The SA/HTI was the poorest at 1260 MPa. It should be noted that composites with the LTO and HTO interphases exhibited lower elastic modulus when compared to their corresponding LTI and HTI counterparts.

The crack densities, ρ_c, in the different specimens tested to failure at room temperature are also shown in Table 2. These were obtained by measurements from polished longitudinal sections after they were exposed to a plasma-etch. The normalized cumulative AE energy was taken to be the relative crack distribution [11]. Multiplying the final measured crack density by the normalized cumulative AE energy enables an estimated, stress-dependent matrix crack density. The non-linear strain is due to the formation of matrix cracks. A relationship for total strain based on the applied stress, σ, and the matrix crack density, ρ_c, has been formulated by Pryce and Smith [12] and Curtin et al. [13] as follows:

$$\varepsilon = \sigma/E_c + \alpha\delta(\sigma)\rho_c/E_f \ (\sigma + \sigma_{th}); \ \text{for } \rho_c^{-1} > 2\delta \quad (4)$$

where E_c and E_f are the elastic moduli of the composite and fiber, respectively, σ_{th} is the residual stress, and the sliding length

$$\delta = \alpha\, r\, (\sigma + \sigma_{th}) / 2\tau \quad (4a)$$

where r is the fiber radius, τ is the interfacial shear stress, and

$$\alpha = (1\text{-}f_o)\, E_m / f_o\, E_c \quad (4b)$$

where f_o is the fraction of fibers in the loading-direction, i.e., f/2. Since the only unknown variable in Equation 4a is τ, Equation 4 can be used to determine a value for τ by best-fitting Equation 4 to the stress-strain curve. Figure 4 shows one example for a HNS composite. The τ-values determined for the different composites tested in this study ranged from 22 to 60 MPa and are listed in Table 2.

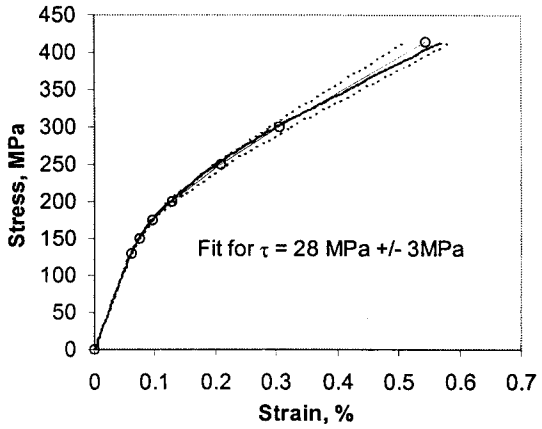

Figure 4: Determination of τ from best-fit stress-strain curve for HNS/BN02. Thick-solid curve is measured tensile stress-strain curve with hysteresis loops removed. Circles represent best fit value and dashed lines represent stress-strain relationship using a τ-value 10% greater and less than the best-fit value.

The fracture surfaces of several specimens were examined and all exhibited good fiber pull-out with the exception of the SA/HTI composite, which exhibited a rather "flat" fracture surface. Of primary interest was the presence of "outside debonding" in the specimens with the LTO and HTO interfaces. The only system that exhibited such behavior was the SA/HTO composite (Figure 5). The SA/LTO composite fracture surface, for the most part, exhibited debonding between the fiber and the interphase, i.e., "inside debonding." The cause for this difference is not clear at this point.

Figure 5: Field-emission scanning electron micrograph of SA/HTO fracture surface showing how BN adhered to fiber surface during pull-out.

815°C Tensile Stress-Rupture Properties

Tensile stress-rupture tests were performed at 815°C in ambient air. Figure 6 shows the rupture data for both fiber-type systems. There is some difficulty in analyzing the results based on absolute stress because the panels were of different thickness and contained different volume fractions of fiber. To compare rupture behavior, the data is also plotted as stress on the fibers if fully loaded (obtained by dividing the absolute stress by f_o for each specimen) in Figure 7. For composites made with the Sylramic fibers and containing different constituent volumes, it has been shown that comparing rupture behavior in terms of the stress carried by the fibers is a good first-order approach [7,14]. It is recognized, however, that stress-rupture of non-oxide composites at intermediate temperature are affected by many other factors including applied stress, environment, the number of exposed cracks, specimen thickness, and the number of fibers, [14]. Also plotted in Figure 7 are data from different fiber-containing MI composite systems tested at NASA under the UEET program. These include a single data-point for a HNS/BN composite-system with a LT Si-doped BN interphase [15], which performed very similarly to the HNS composites tested in this study, and a significant amount of data for Sylramic and a

NASA-treated Sylramic fiber referred to as Syl-iBN MI composite systems. The Syl-iBN possesses an *in situ* BN layer on the fiber after a proprietary treatment [16]. All of the composites referred to from the NASA UEET program were

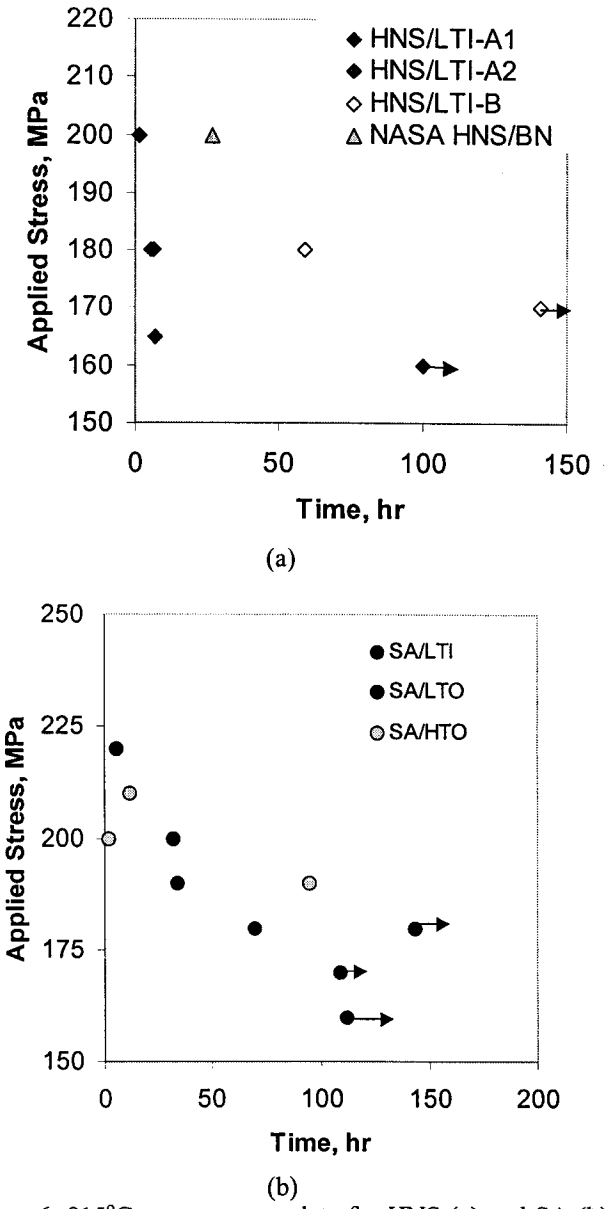

Figure 6: 815°C stress-rupture data for HNS (a) and SA (b) composites.

fabricated by a different vendor.

It is apparent that the baseline SA/LTI composites outperform the baseline HNS/LTI composites when comparing absolute stress on the fibers. When compared to the Sylramic fiber composites, both SA and HNS composites were superior to as-produced Sylramic, although the SA/LTI composites were even comparable to the Syl-iBN composite system.

Based on the results to date in this study, the effect of "outside debonding" on intermediate temperature properties was insignificant. As reported previously, for Syl-iBN composites with "outside debonding", a significant improvement in rupture stress was observed over "inside debonding" composites, especially for rupture times less than 100 hours [7]. That was not observed for the "outside debonding" system, SA/HTO, tested in this study. One explanation for the SA composite rupture behavior was that SA composite rupture occurred at stresses relatively high in proportion to the absolute stress of the composite. This is

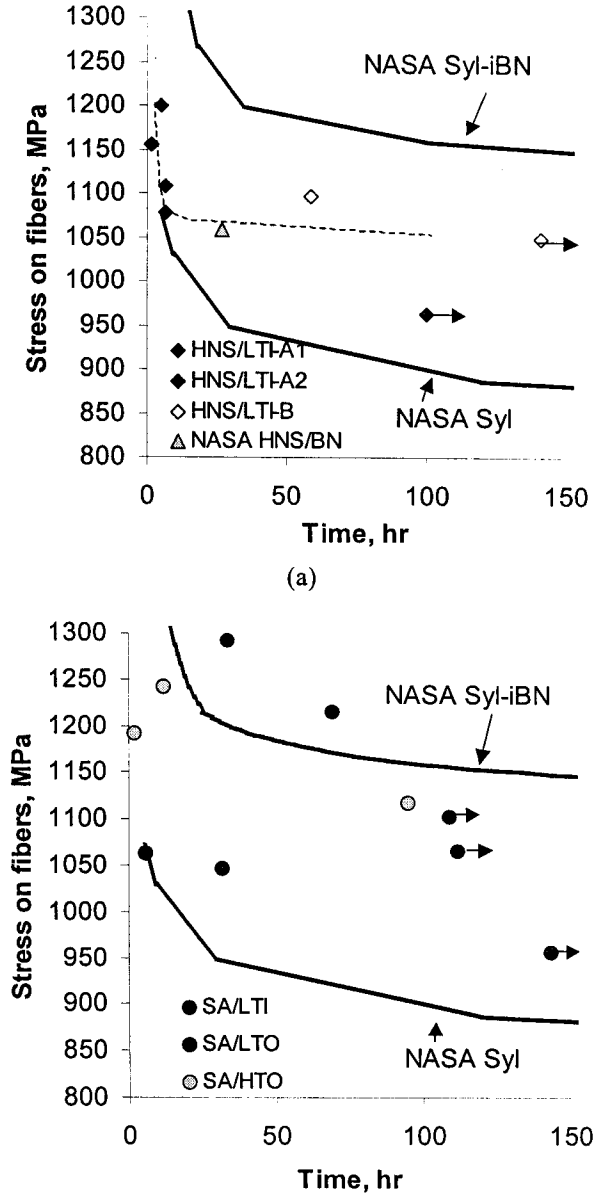

Figure 7: 815°C stress-rupture data plotted as stress on the fibers if fully loaded for (a) HNS and (b) SA

shown in Figure 8 where the fraction of applied rupture stress on the fibers divided by the ultimate stress on the fibers for each composite system is plotted versus rupture time. The HNS and Sylramic composite systems were tested at 45-55% of the room-temperature ultimate strength of the composites; whereas, the SA composites were tested at 65-75% of the room-temperature ultimate strength. The implication is that at

stresses nearer the ultimate stress, a greater number of fibers will fracture during the rupture test due to the statistical nature of fiber failure in and around matrix cracks [14]. As more fiber failure occurs in matrix cracks, the likelihood for fiber-to-fiber interaction leading to catastrophic unbridged-crack growth would be greater and possibly mask any effect of oxidation embrittlement, or lack thereof.

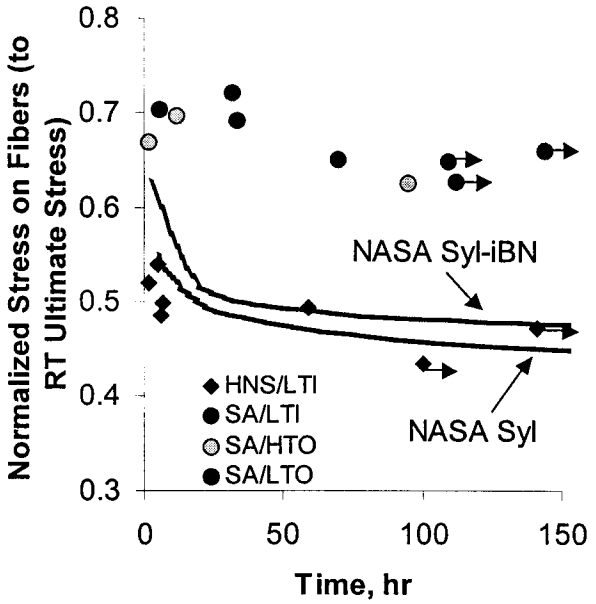

Figure 8: The fraction of RT ultimate stress applied during 815°C rupture versus time.

Table 3: 1315°C Tensile Results

Panel	1315C Fast Fracture Strength, MPa	% 1315C Fast Fracture Strength of RT Strength#	100 hr 1315C creep; 103MPa creep strain,%	100 hr 1315C creep; 103MPa Retained Strength	% Retained Strength of RT Strength#
HNS/LTI-A1	>253*	>74%*	0.09	256	77%
HNS/LTI-A2	>271*	>69%*	0.05	295	72%
HNS/LTI-B	--	--	0.07	255	73%
SA/LTI1	>190*	>68%*	0.06@		
SA/LTI2	--	--		230	83%
SA/LTO1	255	86%	0.04	239	80%
SA/LTO2	--	--			
SA/HTI	>162*	>83%*			
SA/HTO1	219	89%			
SA/HTO2	--	--	0.06	189	> 60%*

calculated from stress on fibers at failure
* Failed well outside of gage section
@Test stopped after 50 hours due to computer malfunction

Oxidation embrittlement was apparent for the SA/LTI composites, but not for the SA/HTO composites. The fracture surfaces of the SA/LTI-2 specimen that failed after 34 hours oxidized significantly. An oxide film was evident on the SiC surface of the fracture surface and the BN interphase at the fracture surface reacted to form an oxide. The SA/LTI-2 specimen showed little pullout, with most of the fibers being fused to one another or to the matrix due to the reaction of the interphase with the environment to form a solid oxidation product. The fracture surface of the SA/HTO specimen that failed after 95 hours, on the other hand, showed relatively minor oxidation. Some oxidation of the matrix surface was evident; but the HTO interphase was for the most part hardly oxidized at all. Also, the fracture surface of the SA/HTO specimen after the stress-rupture testing showed good pullout, and was similar to that of a comparable specimen tested at room temperature. This behavior is identical to that observed for Syl-iBN composites with outside debonding and inside debonding interphases [6]. Therefore, even though the SA/LTI and SA/HTO composites performed similarly at 815°C under stress-rupture, the fact that little oxidation embrittlement was observed for the SA/HTO composite implies that the HTO interphase is more oxidation resistant than the LTI interphase.

It should be noted that for all the data shown in Figures 6 and 7, through-thickness matrix cracking had occurred in all specimens with the exception of the SA/LTI composites tested at the two lower stresses.

1315°C Tensile Properties

Tensile fast fracture, 100-hour creep strain at 103 MPa, and retained strength after 100-hour creep at 103 MPa were performed for most composite systems. Table 3 summarizes the data for all three properties. Unfortunately, failure during fast fracture testing at 1315°C often occurred well outside the gage section as noted in Table 3. However, for the specimens where fracture occurred in the gage section, greater than 85% of the room-temperature ultimate strength was achieved. The creep (time-dependent) strain at 1315°C and 103 MPa was less than 0.1%, comparable to the best Syl-iBN composites tested in the UEET program at NASA. The retained strength of crept specimens was always high, 70 to 80% of the room temperature ultimate strength, and essentially equivalent to the fast-fracture strength at 1315°C. The applied stress for creep was below the matrix cracking stress in all cases. Since little time-dependent strain occurred and high retained strengths were achieved, these indicate a very creep-resistant matrix. One

Table 4: Through-thickness properties

Panel	ILT, MPa	Thermal Conductivity (RT), W/mK	Thermal Conductivity (1000°C), W/mK
HNS/LTI-A1	--	28.2	18.3
HNS/LTI-A2	--	25.5	15.3
HNS/LTI-B	7.2 +/- 0.3	32.8	20.4
SA/LTI1	8.5 +/- 0.4	30.5	19.0
SA/LTI2	10.3 +/- 0.4	--	--
SA/LTO1	--	--	--
SA/LTO2	7.6 +/- 2.4	27.3	17.9
SA/HTI	8.2 +/- 2.1	25.6	18.8
SA/HTO1	9.3 +/- 0.2	29.3	20.5
SA/HTO2	--	--	--
NASA 01/01*	10.7 +/- 5.2	19	15.5
NASA 9/99#	15.5	26.3	16.3

* Sylramic-iBN, MI SiC composite developed under NASA UEET program
# Sylramic, MI SiC composite developed under NASA EPM program

surprising result was that the HNS/LTI-B composite with the higher fraction of Si (HNS/LTI-3) did not have higher relative creep strains than the other two HNS/LTI composites with lower volume fractions of Si.

Through-Thickness Properties

Room temperature interlaminar tensile strength (ILT) and thermal conductivities at room temperature and at 1000°C are shown for a number of different composite panels tested in this study in Table 4. Also shown in Table 4 are the ILT and thermal conductivities measured on composites tested at NASA under the UEET program for two different composite systems containing Sylramic fibers (9/99) and the NASA-treated Syl-iBN fibers (01/01) [17].

The thermal conductivity of the composites in this study proved to be superior to the composites fabricated under the NASA UEET program by another vendor. For HNS/LTI composites, the composite with the highest fraction of fibers, HNS/LTI-A2, had the poorest thermal conductivity, and the panel with the highest silicon content (HNS/LTI-B) had the best conductivity.

CONCLUSIONS

The constituent content of SiC fiber reinforced-MI SiC matrix composites strongly affects composite performance. The baseline HNS composites fabricated in this study with different constituent contents show that the matrix cracking stress and thermal-conductivity are dependent on the relative amounts of composite constituents. Consequently, it is possible to tailor the properties and performance of these composites by controlling the relative volume fractions of fiber, CVI-SiC, slurry and silicon content in the composite to maximize the proportional limits and thermal conductivity for applications at temperatures below 1315°C. The lower as-produced fiber-strength SA fiber composites proved to be superior in intermediate temperature stress-rupture when compared to the HNS composites in this study and very comparable to the state-of-the-art Syl-iBN composites tested in the NASA UEET program. This implies that for applications where a component experiences tension at intermediate temperatures (600 to 1000°C), SA fiber composites may perform better despite their lower strength. Finally, the interlaminar strengths of the composites tested in this study were slightly worse than those tested for Sylramic and Syl-iBN composites fabricated by a different vendor and tested under the NASA UEET program. However, the thermal conductivity of the composites were superior. Obviously, the causes of these two observations need to be quantified so that the former can be improved while the latter is not diminished.

ACKNOWLEDGMENTS

This work was supported by an internally funded technology development program at Goodrich Corporation and the UEET program at NASA Glenn Research Center. The authors would like to acknowledge J. A. DiCarlo at NASA-Glenn, and M. Purdy, T. Nixon and S.K. Lau at Goodrich for their expertise and insight on CMC properties and processing. We thank Lanny Ritz, Jaime Alvarado, Jeff Lewis and Bob Dietz for their assistance with processing and characterization. Finally, we wish to thank A. Misra at NASA-Glenn and P. Walsh, , S. Shanmugham and R. Hines at Goodrich for many useful comments and discussions.

REFERENCES

1. Brewer, D., 1999, "HSR/EPM Combustor Materials Development Program," Mater. Sci. Eng., Vol. A261, pp. 284-291.
2. M. Verrilli, Robinson, R.C., Calomino, A.M., and Thomas, D.J., "Ceramic Matrix Composite Vane Subelement Testing in a Gas Turbine Environment," ASME Paper GT2004-53970, Proceedings of ASME Turbo Expo 2004, June 14-17, 2004, Vienna, Austria
3. Kimmel, J., Price, J., More, K., Tortorelli, P., Linsey, G., and Sun, E., "The Evaluation of CFCC Liners After Field Testing in a Gas Turbine – IV," Paper GT-2003-38920, Proceedings of ASME Turbo Expo 2003, June 16-19, 2003, Atlanta, Georgia, USA
4. Dean, A.J., Corman, G.S., Bagepalli, B., Luthra, K.L., DiMascio, P.S., and Orenstein, R.M., 1999, "Design and Testing of CFCC Shroud and Combustor Components," 99-GT-235.
5. DiCarlo, J.A., Yun, H.M., Morscher, G.N., and Bhatt, R.T., "Progress in SiC/SiC Development for Gas Turbine Hot-Section Components Under NASA EPM and UEET Programs," ASME Paper GT-2002-30461, Proceedings of ASME Turbo Expo 2002, June 3-6, 2002, Amsterdam, The Netherlands.
6. Morscher, G.N., Yun, H.Y., and Hurwitz, F.I., "High Temperature Si-doped BN Interphases for Woven SiC/SiC Composites," Ceram. Eng. Sci. Proc., Vol. 23, No. 3, pp. 379-386 (2002)
7. G.N. Morscher, H.M. Yun, J.A. DiCarlo, and L. Thomas-Ogbuji, "Effect of a BN Interphase that Debonds Between the Interphase and the Matrix in SiC/SiC Composites," *J. Am. Ceram. Soc.*, in print
8. Hasselman, D.P.H., private communication.
9. M. Steen and J.L. Valles, ASTM STP 1309, M.G. Jenkins et al., Eds. American Society for Testing and Materials, West Conshohocken, PA, 1997, pp. 49-65
10. Morscher, G.N., 2000, "Modal Acoustic Emission Source Determination in Silicon Carbide Matrix Composites," CP509, *Review of Progress in Quantitative Nondestructive Evaluation*, eds. D.O. Thompson and D.E. Chimenti, American Institute of Physics, pp. 383-390.
11. G.N. Morscher, Stress-Dependent Matrix Cracking in 2D Woven SiC-fiber Reinforced Melt-Infiltrated SiC Matrix Composites, *Comp. Sci. Tech.*, in print
12. A.W. Pryce and P.A. Smith, *Br. Ceram. Trans.*, Vol. 92, No. 2 (1993) 49-54.
13. W.A. Curtin, B.K. Ahn, and N. Takeda, *Acta mater.*, Vol. 46, No. 10, (1998) pp. 3409-3420.
14. G.N. Morscher and J.D. Cawley, "Intermediate Temperature Strength Degradation in SiC/SiC Composites," *J. European Ceram. Soc.*, vol. 22 (2002) 2777-2787.
15. G.N. Morscher, Unpublished data.
16. H.M. Yun and J.A. DiCarlo, "Comparison of the Tensile, Creep, and Rupture Strength Properties of Stoichiometric SiC Fibers," *Cer. Eng. Sci. Proc.*, **20** [3] 259-272 (1999)
17. Calomino, A., Presented at Ultra Efficient Engine Technology Program Technology Forum, October 2002